Control Methodology to Mitigate the Grid Impact of Wind Turbines

Barry G. Rawn, *Student Member, IEEE*, Peter W. Lehn, *Senior Member, IEEE*, and Manfredi Maggiore, *Member, IEEE*

***Abstract*—This paper introduces a new control topology for converter-interfaced wind turbines. Through a singular perturbation decomposition of the system dynamics, a controller is designed that isolates wind-power fluctuations from the power grid. Specifically, the controller causes the closed-loop wind turbine to behave as a simple first-order power filter, where power injected into the grid is a low-pass filtered version of the incident wind power. It is shown that a turbine hub-speed instability imposes a limit on the largest filtering time constant that may be safely implemented. A linearized analysis is used to calculate how a small filter time constant can be implemented to obtain regulation of the tip-speed ratio for the widest range of frequencies. The methodology thus offers the possibility to either deliver a filtered power at suboptimal conversion efficiency or track peak wind power. It is mathematically demonstrated that the control structure achieves the regulation of torsional dynamics and the dc-link capacitor voltage without involving the grid-side converter controls, thus eliminating the influence of those dynamics on the grid. Simulation studies are used to demonstrate the methodology's viability and explore the associated tradeoffs.**

***Index Terms*—Dynamics, energy storage, power-generation control, wind-power generation.**

I. Introduction

In many areas of the world, significant contributions by wind-energy conversion systems to the generation mix are planned. Compliance with new grid codes [1] and contribution to system regulation by wind farms [2], [3] are being studied. It has been commented that the sacrifice of energy capture in order to obtain better control of wind farm power output may become more common [1], [4]. However, in most installations and published research, the power delivered to the grid is a consequence of the primary goals of tip-speed regulation, shaft damping, and dc-link capacitor voltage regulation. Grid power is therefore a *system output* that can contain fast variations caused by the excitation of conversion system modes by wind turbulence. This complicates studies of grid impact.

This paper presents a control structure for a system with a fully rated converter, where the power delivered to the grid is defined as a *control input* $P_{\rm ref}$. An analytical separation into fast and slow time-scale models is central to the approach. It is first shown that the variations of the shaft, generator speed and capacitor voltage constitute a fast subsystem that can be regulated without exchanging energy with the grid. The stability implications of imposing a desired power extraction $P_{\rm ref}$ on the more slowly evolving turbine hub are then examined.

The control structure is used to implement a methodology, where $P_{\rm ref}$ is based on wind speed, to deliver a filtered version of the available power. The slow time-scale model is analyzed in conjunction with the wind models to gain insight into the bounds on the implementable time constant. The concept of employing turbine kinetic energy to absorb fluctuations and deliver a derated, filtered power has also been studied in [5] and [6]. In these approaches, as well as in the one proposed here, a tradeoff of filtered power for decreased energy capture and increased speed variations must be accepted. Simulation results quantify this tradeoff and demonstrate the isolating properties of the control structure.

Manuscript received August 2, 2005; revised March 1, 2006. Paper no. TEC-00262-2005.

The authors are with Edward S. Rogers Sr. Department of Electrical and Computer Engineering, University of Toronto, Toronto, ON M5S 3G4, Canada (e-mail: barry.rawn@utoronto.ca; lehn@ecf.utoronto.ca; maggiore@control.utoronto.ca).

Digital Object Identifier 10.1109/TEC.2006.878242

II. Modeling and System Structure

A useful model must include the characteristic frequency content of wind speeds, the static curve that describes the aerodynamic conversion of energy by the bladed turbine rotor, and a dominant mechanical mode between the inertia of the rotor and the generator mass. In this paper, a wind turbine with parameter values as in [7], interfaced through a back-to-back converter system, has been studied.

A. Wind Modeling

Over periods shorter than an hour, wind speed can be approximated as the superposition of a slowly varying mean speed $\bar{v}_w$ and N sinusoidal components having amplitudes A_i and random phases ψ_i

$$v_w(t) = \bar{v}_w + \sum_{i=0}^{N} A_i \cos(\omega_i t + \psi_i). \tag{1}$$

The frequencies ω_i and amplitudes A_i of these N components are given by an empirically determined spectral density function. For this paper, the von Karman distribution [8] is used

$$S_{vv}(\omega_i) = \frac{0.475\sigma^2(L/\bar{v}_w)}{[1+(\omega_i L/\bar{v}_w)^2]^{5/6}}. \tag{2}$$

The distribution (2) depends on the mean speed $\bar{v}_w$, the roughness of the surrounding landscape (as described by a characteristic length scale L), and the standard deviation σ of wind speeds. The frequencies ω_i are chosen to be logarithmically spaced in order to properly represent the frequency content of (2). The amplitude A_i of each discrete frequency component is chosen to give it a power equal to that contained in a certain frequency

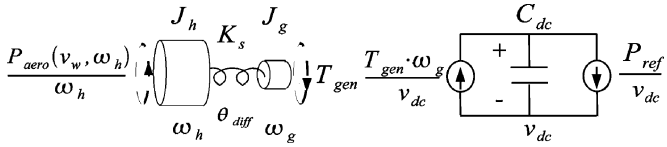

Fig. 1 Schematic representation of the system model showing parameters and states.

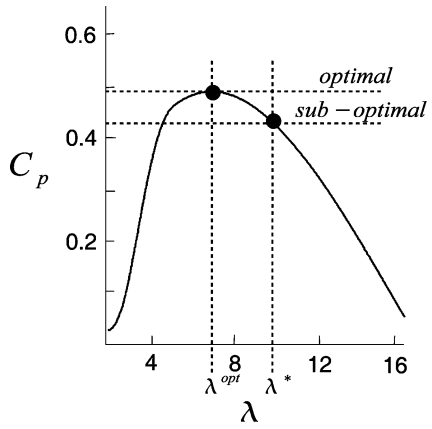

Fig. 2. C_P curve. Suboptimal efficiency occurs for $\lambda^* > \lambda^{\rm opt}$.

band, which is found by calculating the area under the density function $S_{vv}(\omega_i)$. The amplitude is given as follows:

$$A_i(\omega_i) = \sqrt{2 \times \frac{[S_{vv}(\omega_i) + S_{vv}(\omega_{i+1})][\omega_{i+1} - \omega_i]}{2}}. \quad (3)$$

B. Conversion System Modeling

The power coefficient, C_P, describes the efficiency with which wind energy is extracted by the turbine blades. C_P depends on the tip-speed ratio λ defined as

$$\lambda = \frac{R\omega_h}{v_w} \quad (4)$$

where ω_h is the rotational speed of the rotor, v_w is the wind speed, and R is the radius of the rotor. C_P (shown in Fig. 2) determines the aerodynamic power $P_{\rm aero}$ extracted from the available wind power

$$P_{\rm aero} = \frac{1}{2}\rho\pi R^2 C_P(\lambda) v_w^3. \quad (5)$$

The shape of the C_P curve causes maxima in both the speed–power and speed-torque curves. Maximum power is obtained when $\lambda = \lambda^{\rm opt}$ as shown in Fig. 2.

This aerodynamic relation determines the dynamics of the turbine rotor speed ω_h and depends on the dimensionless ratio λ, rather than the wind speed or rotor speed individually. Operation can occur at a suboptimal conversion efficiency around a tip-speed ratio $\lambda^* > \lambda^{\rm opt}$.

The mechanical components of a wind turbine system are commonly simplified to a two-mass model with a flexible coupling having stiffness K_s [9], [10]. In the implementation chosen for this paper, these elements are cascaded through an ac–dc–ac converter as shown in Fig. 1. Through the application of vector controls for the machine-side converter currents, the electromagnetic torque and flux inside the generator can be controlled with a high bandwidth [11]. Therefore, it is assumed that the torque $T_{\rm gen}$ established in the generator is a control input. The flux is simply set constant at $\Phi_{\rm rated}$. The active and reactive power leaving the grid-side converter can also be regulated using high-bandwidth vector controls. The active power is chosen as an independent control input $P_{\rm ref}$, and reactive power $Q_{\rm ref}$ can be specified as desired. The converter is thus simplified to a differential equation for the dc-link capacitor voltage, where the control inputs $T_{\rm gen}$ and $P_{\rm ref}$ enter as dictated by the power balance.

The uncontrolled state–space system associated with Fig. 1 is as follows:

$$\begin{aligned}
\frac{d\omega_h}{dt} &= \frac{1}{J_h}[P_{\rm aero}(v_w(t), \omega_h)/\omega_h - K_s\theta_{\rm diff}] \\
\frac{d\theta_{\rm diff}}{dt} &= \omega_h - \omega_g \\
\frac{d\omega_g}{dt} &= \frac{1}{J_g}(K_s\theta_{\rm diff} - T_{\rm gen}) \\
\frac{dv_{\rm dc}}{dt} &= \frac{T_{\rm gen}\omega_g - P_{\rm ref}}{C_{\rm dc}v_{\rm dc}}
\end{aligned} \quad (6)$$

where $T_{\rm gen}$ and $P_{\rm ref}$ are the control inputs, $v_w(t)$ is a time-varying wind-speed input signal, and other symbols are as defined in Fig. 1.

C. System Analysis

Because of the large value of J_h, (6) have a singularly perturbed form indicating that their dynamics take place on two distinct time scales. For analysis and control design, (6) can be formally separated into two independent subsystems of equations.

The separation proceeds by assuming that the faster states of the system are stable and settle to steady-state values. This simplifies the influence of the fast states on the slow state. The control input $T_{\rm gen}$ is defined as having a slow component $\bar{T}_{\rm gen}$, and a fast component $\tilde{T}_{\rm gen}$ that is zero at steady state

$$T_{\rm gen} = \bar{T}_{\rm gen} + \tilde{T}_{\rm gen}. \quad (7)$$

By setting the left-hand side of the last three equations of (6) to zero, quasi-steady-state values for $\theta_{\rm diff}, \omega_g$, and the slow control input $\bar{T}_{\rm gen}$ can be found as

$$\begin{aligned}
\theta_{\rm diff} &= \frac{\bar{T}_{\rm gen}}{K_s} \\
\omega_g &= \omega_h \\
\bar{T}_{\rm gen} &= \frac{P_{\rm ref}}{\omega_g}.
\end{aligned} \quad (8)$$

The above conditions correspond to a lack of torsional oscillations and power balance across the converter. The quasi-steady-state dc voltage $\bar{v}_{\rm dc}$ is unspecified by (8) and can be freely assigned. The quasi-steady-state values, which vary on a slow time scale, are substituted in the first equation of (6) to obtain a slow subsystem with a single state $\bar{\omega}_h$, time-varying input $v_w(t)$,

and control input $P_{\rm ref}$ as

$$\frac{d\bar{\omega}_h}{dt} = \frac{P_{\rm aero}[v_w(t), \bar{\omega}_h] - P_{\rm ref}}{J_h \bar{\omega}_h}. \tag{9}$$

The fast dynamics of (6) are viewed as evolving on their own time scale $\tau = J_h t$. On this time scale, it is assumed that the state ω_h changes so slowly that it can be replaced with a constant ξ_0. Defining

$$\begin{bmatrix} y_1 \\ y_2 \\ y_3 \end{bmatrix} = \begin{bmatrix} \theta_{\rm diff} - \frac{1}{K_S}\frac{P_{\rm ref}}{\omega_g} \\ \omega_g - \omega_h \\ v_{\rm dc} - \bar{v}_{\rm dc} \end{bmatrix} \tag{10}$$

the substitution

$$T_{\rm gen} = \frac{P_{\rm ref}}{\omega_g} + \tilde{T}_{\rm gen} \tag{11}$$

into the last three equations of (6) yields the dynamic equations of the fast subsystem

$$\begin{aligned} \frac{dy_1}{d\tau} &= -y_2 \\ \frac{dy_2}{d\tau} &= \frac{1}{J_g}(K_s y_1 - \tilde{T}_{\rm gen}) \\ \frac{dy_3}{d\tau} &= \frac{\xi_0 + y_2}{C_{\rm dc}(\bar{v}_{\rm dc} + y_3)}\tilde{T}_{\rm gen}. \end{aligned} \tag{12}$$

The control input in (12) is $\tilde{T}_{\rm gen}$. Equations in (12) may be used exclusively for the study of fast dynamics, while (9) is used for the study of slow dynamics, which may be interpreted as the motion of the system's center of inertia.

III. Control Methodology

A. Control Input $T_{\rm gen}$

The two components of the control input $T_{\rm gen}$ are constructed as shown in Fig. 3. By setting $\bar{T}_{\rm gen}$ according to (8), an average power balance is achieved across the back-to-back converter. The component $\tilde{T}_{\rm gen}$ is designed to damp torsional and capacitor voltage oscillations contained in the fast subsystem (12). While (12) is nonlinear, it is only weakly so. This becomes evident from substituting the control law of Fig. 3

$$\tilde{T}_{\rm gen} = \frac{\bar{v}_{\rm dc} + y_3}{\xi_0 + y_2}(-K_1 y_3 - K_2 y_2) \tag{13}$$

where K_1 and K_2 are positive gains. From the approximation $\xi_0 + y_2 \approx \xi_0$ and algebraic manipulation, the following is obtained:

$$\begin{bmatrix} \frac{y_1}{d\tau} \\ \frac{y_2}{d\tau} \\ \frac{y_1}{d\tau} \end{bmatrix} = \begin{bmatrix} 0 & -1 & 0 \\ \frac{K_s}{J_g} & \frac{1}{J_g}\frac{\bar{v}_{\rm dc}}{\xi_0}K_2 & \frac{1}{J_g}\frac{\bar{v}_{\rm dc}}{\xi_0}K_1 \\ 0 & -\frac{1}{C_{\rm dc}}K_2 & -\frac{1}{C_{\rm dc}}K_1 \end{bmatrix} \begin{bmatrix} y_1 \\ y_2 \\ y_3 \end{bmatrix} + \begin{bmatrix} 0 & & \\ & +\frac{1}{J_g\xi_0}K_2 y_3 y_2 & +\frac{1}{J_g\xi_0}K_1 y_3^2 \\ -\frac{1}{C_{\rm dc}\xi_0}K_2 y_2^2 & -\frac{1}{C_{\rm dc}\xi_0}K_1 y_3 y_2 & \end{bmatrix} \tag{14}$$

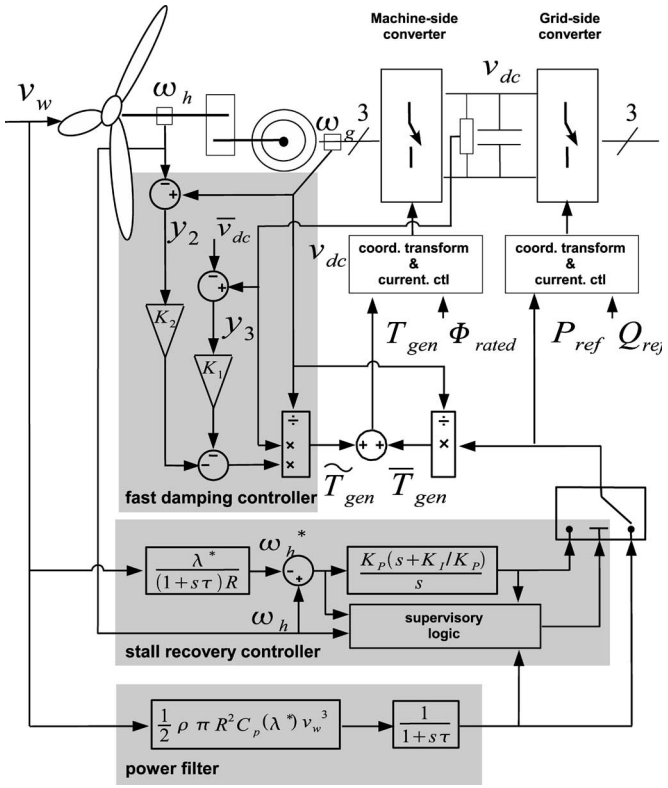

Fig. 3. Full-converter-interfaced wind turbine with control structure.

which has the form of a linear system $\dot{x} = Ax$ with a perturbation $g(x)$

$$\dot{x} = Ax + g(x) \tag{15}$$

that vanishes at the origin of the transformed system, which in this case corresponds to the quasi-steady-state values of $\theta_{\rm diff}, \omega_g$, and $v_{\rm dc}$. The perturbation $g(x)$ has a higher order, so it does not affect the linearization. Hence, if the linear part of the system is stable through appropriate choice of K_1 and K_2, then the origin of the boundary system is locally exponentially stable [12].

Influence of the torsional dynamics and dc-link dynamics on the grid through delivered active power is eliminated by using the generator torque $T_{\rm gen}$ to achieve damping. The energy required to regulate these variations is exchanged with the turbine hub rather than with the grid. No interturbine or turbine-grid modes can ever exist in the proposed controller.

B. Control Input $P_{\rm ref}$

The control input $P_{\rm ref}$ and external input $P_{\rm aero}$ influence the speed $\bar{\omega}_h$ of the turbine hub's center of inertia according to (9). These slow dynamics are common to all converter-interfaced wind turbines.

$P_{\rm ref}$ could be chosen arbitrarily, provided it does not exceed the available power for too long. Ideally, it is desired to demand a filtered power [5], [6] or a power based on grid variables [2], [3], [13]. The torque–speed curves associated with such goals must be examined carefully because they introduce the possibility

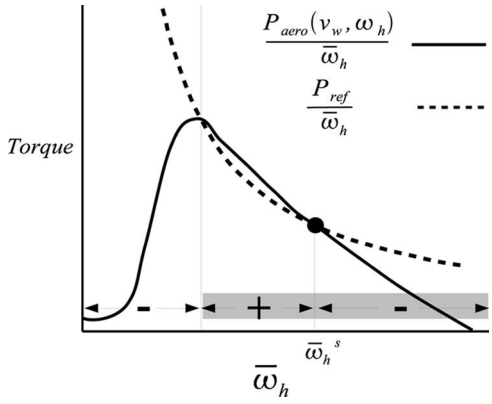

Fig. 4. Torque–speed characteristic for constant power extraction. Sign of net torque (+accelerating, −decelerating) is marked. A stable interval (shaded) of restoring torque exists for the operating point $\bar{\omega}_h^s$.

of instability. A power command $P_{\rm ref}$, which changes more slowly than does turbine hub speed, will produce a generator torque approaching that of a constant power characteristic as in Fig. 4.

Fig. 4 plots the aerodynamic torque and generator torque for the case of constant wind speed and a constant power $P_{\rm ref}$ that is less than the maximum available wind power. An equilibrium is reached at the speed $\bar{\omega}_h^s$, where exactly $P_{\rm ref}$ is being extracted from the wind. For a range of lower speeds, more than $P_{\rm ref}$ is available from the wind, causing an accelerating torque that drives the hub speed back toward $\bar{\omega}_h^s$. Variations of the wind can change the size of this region of restoring torque, and even eliminate it. Maintaining a constant $P_{\rm ref}$ in the presence of such variations may cause instability. Derating $P_{\rm ref}$ to be less than the available power increases the domain of stability of the turbine hub. This can be illustrated by studying a simple example.

Choose a constant power $P_{\rm ref}$ based on a mean wind speed $\bar{v}_w$ as follows:

$$P_{\rm ref} = \frac{1}{2}\rho\pi R^2 C_P(\lambda^*)\bar{v}_w^3 \tag{16}$$

$$\lambda^* \geq \lambda^{\rm opt}, C_P(\lambda^*) \leq C_P(\lambda^{\rm opt}). \tag{17}$$

Choosing $\lambda^* = \lambda^{\rm opt}$ extracts a maximum power, while a higher λ^* extracts a derated power.

Now, let the wind have a simple periodic variation around $\bar{v}_w$, with a period T, as shown in Fig. 5(a). The two aerodynamic torque characteristics corresponding to $v_{w_{\max}}$ and $v_{w_{\min}}$ in the speed–torque plane are shown in Fig. 5(b). The generator torque given by $P_{\rm ref}/\bar{\omega}_h$ is also plotted. From the upper curve, we identify a critical speed $\bar{\omega}_h^u$. No accelerating torque exists below this speed for any portion of the period T. Therefore, if $\bar{\omega}_h$ drops below this speed, it will collapse toward zero.

The trajectory of the operating point is shown in Fig. 5(b) for the case where the maximum power available at wind speed $\bar{v}_w$ is demanded by choosing $\lambda^* = \lambda_{\rm opt}$. The period T is short enough such that the turbine never settles at a constant speed. No region of accelerating torque exists during the interval of low wind speed. However, the wind speed increases before $\bar{\omega}_h$ drops below $\bar{\omega}_h^u$, and therefore the given wind input provokes a stable cycle for the chosen constant power.

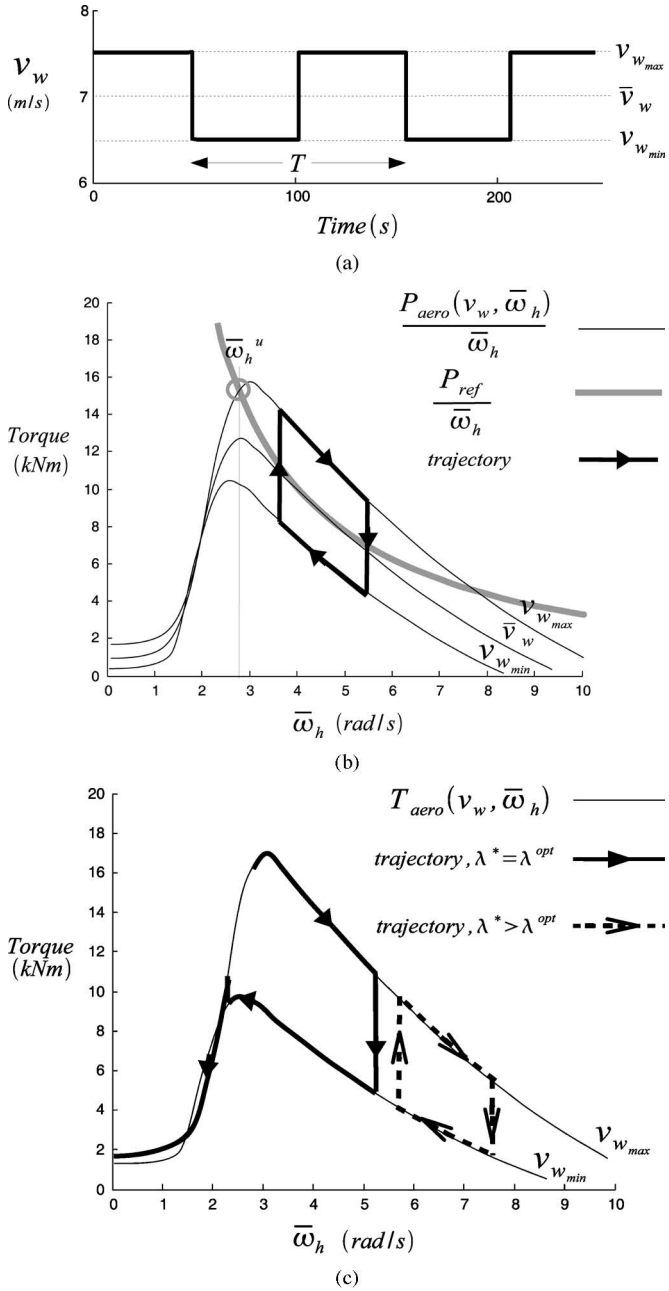

Fig. 5. Dynamics of constant power extraction for square-wave periodic wind input. A larger, slower wind variation provokes a collapse of hub speed when an excessive average power level is demanded. (a) A simple periodic wind-speed input varying between $v_{w_{\max}}$ and $v_{w_{\min}}$ with period T. $\bar{v}_w = 7$ m/s, $T = 105$ s. (b) Response of turbine hub to wind input for constant power extraction equal to the optimal power at $\bar{v}_w$. (c) Response to slower, larger wind variation for optimal power (solid) and derated power (dashed) cases.

In Fig. 5(c), the period and amplitude of the wind input have been increased. The response of the turbine is shown for a power based on $\lambda^* > \lambda_{\rm opt}$ (dashed) in addition to that based on $\lambda = \lambda^{\rm opt}$ (solid). In each case, the excursion of the turbine hub speed is larger because a larger energy variation must now be absorbed. In the case of the power based on $\lambda^{\rm opt}$ (solid line), the wind

variation causes a period of hub deceleration long enough that the hub speed dips below $\bar{\omega}_h^u$. Hence, a collapse of the hub speed is unavoidable. The trajectory associated with the power level based on $\lambda^* > \lambda^{\rm opt}$ (dashed line) remains stable.

IV. Application to Power Filtering

It is clear that stability will limit the duration and size of an arbitrary power demand. Over long periods of time, the power demanded must be chosen to follow the slow variations of the wind resource. The example of Section III-B can be viewed as an approximation of the situation where changes in the mean wind speed are being tracked, but faster fluctuations must be absorbed. The stored kinetic energy of the turbine hub can be employed to further contain fluctuations in the available wind power, in addition to absorbing torsional fluctuations. It has been demonstrated that considerable smoothing of output power can be obtained by derating the demanded power [5]. In this section, the bounds placed on safe operation as a power filter are demonstrated by simulation and explained through analysis of the models of Section I. Guidelines for the design of the power filter time constant and derating are obtained, and performance is reported in Section V.

The output power $P_{\rm ref}$ is chosen to be based on a wind-speed measurement and an adjustable derating $C_P(\lambda^*)$, filtered with a time constant τ

$$\dot{P}_{\rm ref} = \frac{1}{\tau}\left[\frac{1}{2}\rho\pi R^2 C_P(\lambda^*) v_w^3 - P_{\rm ref}\right]$$
$$\lambda^* \geq \lambda^{\rm opt}, \quad C_P(\lambda^*) \leq C_P(\lambda^{\rm opt}). \tag{18}$$

It is necessary to provide a control structure that guarantees stable operation in all conditions. If instability does occur, it is detected by the supervisory logic block in the *stall recovery controller* shown in Fig. 3, and $P_{\rm ref}$ is specified by a speed regulator instead of the power filter. $P_{\rm ref}$ then varies to stabilize a reference turbine hub speed ${\omega_h}^*$, which is a low-pass filtered version of $\frac{\lambda^*}{R} v_w(t)$. When the power level specified by the speed regulator enters a suitable neighborhood of the level being specified by the power filter, the supervisory control reverts $P_{\rm ref}$ to the power-filter signal from (18).

Robust detection of instability can be based on the simultaneous satisfaction of several conditions related to the operating point and its dynamics that are as follows:

1) decreasing turbine hub speed;
2) decrease of $\lambda(t)$ below a threshold;
3) increase of the derivative $\partial \bar{T}_{\rm gen}/\partial \bar{\omega}_h$ above a threshold.

The speed regulator is the following simple proportional integral feedback controller:

$$P_{\rm ref} = K_P(\bar{\omega}_h - \bar{\omega}_h^*) + K_I \eta$$
$$\dot{\eta} = \bar{\omega}_h - \bar{\omega}_h^* \tag{19}$$

where $\bar{\omega}_h^*$ is determined by the filtered wind speed and λ^* as shown in Fig. 3. At the instant t_0 when a switch of control is made, the continuity of $P_{\rm ref}$ [i.e., $P_{\rm ref}({t_0}^+) = P_{\rm ref}({t_0}^-)$] is assured by initializing the integral state η appropriately.

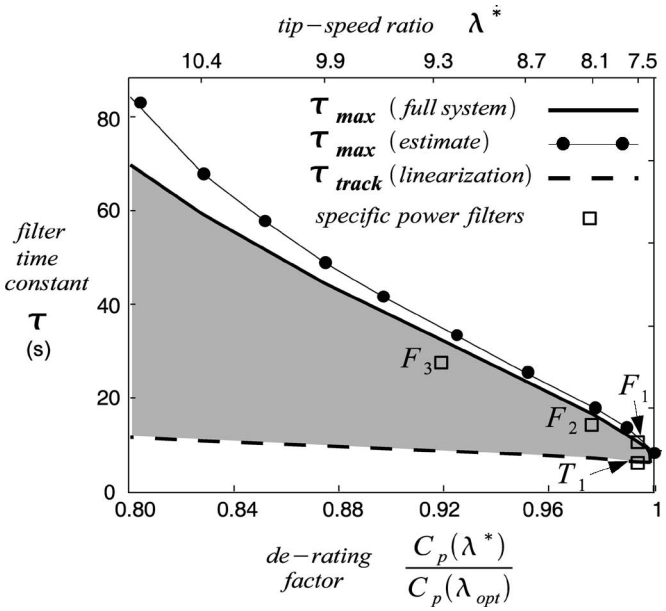

Fig. 6. Operating envelope of the power filter. Maximum filter time constant $\tau_{\rm max}$ (solid) and minimum filter time constant $\tau_{\rm track}$ (dashed) for a given derating and corresponding tip-speed ratio λ^* are shown. Certain filters F_3–F_1 and T_1 are selected to demonstrate performance in Section V.

A. Stability Threshold

The response of the full nonlinear system (6) to a 70-min time series of measured wind speed was simulated over a wide range of parameters λ^* and τ. For each pair, state variables were monitored for instability. A maximum tolerable time constant $\tau_{\rm max}$ was defined as the largest τ for which no interventions by the supervisory control occurred. Fig. 6 shows the dependence of $\tau_{\rm max}$ on the derating of $P_{\rm ref}$. The stability threshold places an upper bound on the operating envelope of the system. A rough estimate of the threshold (also shown in Fig. 6) can be produced using a simpler method based on a single representative sinusoidal wind speed and the slow subsystem (9). The approximations that yield this estimate provide some insight into the system, but must be used with caution. The method is derived from the study of a linearization of (9), which gives further guidance on the selection of τ and λ^*.

B. Filter Design From Linearization

A linearized model of the speed $\bar{\omega}_h$ is obtained by substituting (18) in (19), linearizing at a stable operating point $v_w^{\rm op} = \bar{v}_w$, $P_{\rm ref} = 1/2\rho\pi R^2 C_P(\lambda^*)\bar{v}_w^3$, $\bar{\omega}_h^{\rm op} = (\lambda^*/R)\bar{v}_w$, and taking Laplace transforms. This yields a single-input, single-output transfer function $G(s)$ from the wind speed to the turbine hub speed

$$\Delta\bar{\omega}_h = G(s)\Delta v_w$$
$$= \frac{\lambda^*}{R}\frac{[1+(s/\omega_{\rm zero})]}{[1+(s/\omega_{\rm pole})][1+(s/\omega_{\rm filt})]}\Delta v_w \tag{20}$$

where

$$\omega_{\rm filt} = \frac{1}{\tau} \tag{21}$$

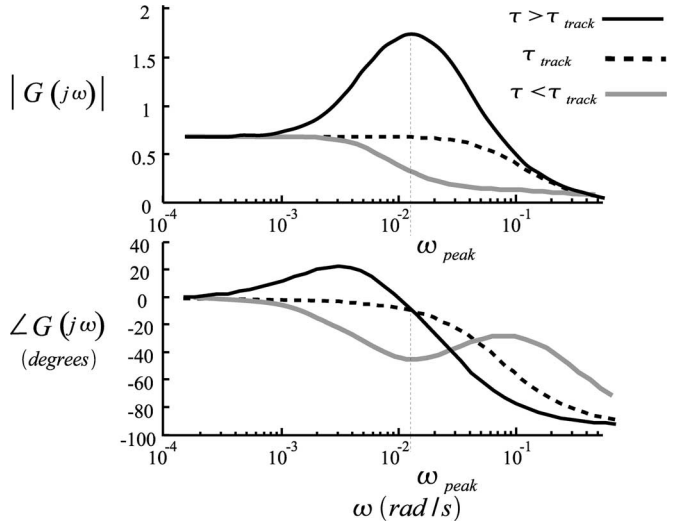

Fig. 7. Bode plots of the transfer function $G(j\omega)$ for different filter time constants τ. For $\tau = \tau_{\rm track}$, the closest possible tracking of λ^* occurs. For $\tau > \tau_{\rm track}$, filtering and large λ variations occur due to a resonant peak at $\omega_{\rm peak}$.

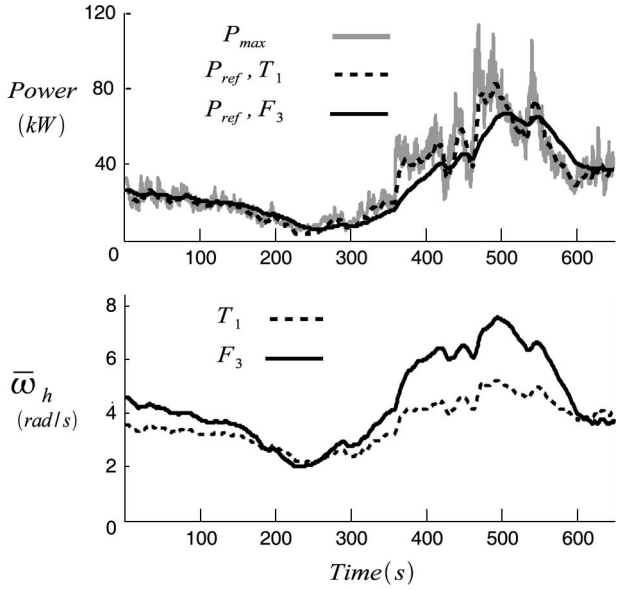

Fig. 8. Power filtering (F_3) and power tracking (T_1) modes, compared against available wind power $P_{\rm max}$. Speed variations are broader for the parameter pair F_3 and a smoother power is delivered.

$$\omega_{\rm zero} = \omega_{\rm filt} \frac{1}{1 + \frac{3C_P(\lambda^*)}{\left(-\frac{dC_P}{d\lambda}|_{\lambda^*}\right)\lambda^*}} \tag{22}$$

$$\omega_{\rm pole} = \frac{\rho \pi R^3}{2J_h} \frac{{v_w^{\rm op}}^2}{\bar{\omega}_h^{\rm op}} \left(- \left. \frac{dC_P}{d\lambda} \right|_{\lambda^*} \right). \tag{23}$$

The dc gain of the Bode plots shown in Fig. 7 is determined by the desired tip-speed ratio λ^*. Perfect regulation of the desired tip-speed ratio (i.e., power tracking) would result in a Bode plot with gain λ^*/R and a phase of 0° at all frequencies. The power filter introduces the left-half plane zero and pole $\omega_{\rm zero}$ and $\omega_{\rm filt}$, which have important effects on the response of the turbine hub speed. For small τ, the power filter has little effect and the time constant $\omega_{\rm pole}$ of the turbine hub dominates the response, as shown by the gray line in Fig. 7.

For a unique filter time constant $\tau_{\rm track}$, the natural response of the turbine hub is compensated by $\omega_{\rm zero}$, generating a first-order response that maintains the gain close to its dc value up to $1/\tau$. This value of τ produces tracking for the largest range of frequencies possible; it can be immediately obtained from (22) and (23).

As τ increases beyond $\tau_{\rm track}$ (solid dark line in Fig. 7), the model develops a resonant peak at a frequency $\omega_{\rm peak}$. The phase-leading response has the physical explanation that the hub-speed response to wind variations is larger than that necessary to maintain the tip-speed ratio λ^*, and that absorption of wind fluctuations is occurring.

The linear system (20) cannot capture the instability that gives rise to the threshold time constant $\tau_{\rm max}$, but it provides the resonant frequency $\omega_{\rm peak}$ of a given operating point. To produce an estimate of $\tau_{\rm max}$, it is assumed that the crucial response of the speed $\bar{\omega}_h$ occurs at this frequency. The wind-speed input is therefore simplified to a mean speed and a single sinusoidal component as

$$v_w(t) = \bar{v}_w + V_w \cos(\omega_{\rm peak} t). \tag{24}$$

This representative sinusoidal signal should have the same power as the frequency components of wind that may affect stability by causing deviations in tip-speed ratio. The resonant hump of (20) shows the frequency range of concern, and the power spectral density (2) describes the power in a given range. Therefore, the amplitude V_w is based on the area under (2) at frequencies greater than the beginning of the resonant hump of (20)

$$V_w \approx \sqrt{2 \int_{\omega_{\rm zero}/2}^{\infty} S_{vv}(\omega_i)\, d\omega} \tag{25}$$

where the integral is discretely approximated.

When the slow subsystem (9), with control input (18) and wind input (24), is simulated for a set of initial conditions, the turbine hub speed either collapses or settles to a limit cycle for each one. Further study of this simplified nonlinear system could produce an analytical result on how the existence of a stable limit cycle depends on the parameter τ. Iterative simulations were used to construct the estimate of $\tau_{\rm max}$ shown in Fig. 6.

For each conversion efficiency $\lambda^* \geq \lambda^{\rm opt}$, the filter time constants $\tau_{\rm track}$ and $\tau_{\rm max}$ define an operating envelope for the conversion system that ranges between tracking of λ^* and the absorption of wind-power fluctuations. The operating envelope is the shaded region in Fig. 6. Any tradeoff between maximizing energy capture $(\lambda^{\rm opt}, \tau_{\rm track})$ and delivering smooth power $(\lambda^* > \lambda^{\rm opt}, \tau_{\rm max})$ can easily be selected. Several pairs of parameters (marked as F_3, F_2, F_1, and T_1) have been selected as examples of possible filters to be evaluated in Section V.

TABLE I
SUMMARY: ENERGY CAPTURE AND SPEED VARIATIONS IN THE FILTERING MODE

	Energy Capture(%)	τ (s)	Average Hub Speed (rad/s)	Std. Dev (rad/s)
T_1	99.4	6	3.72	0.42
F_1	99.3	11	3.69	0.65
F_2	97.6	16	3.99	0.80
F_3	91.5	28	4.57	1.01

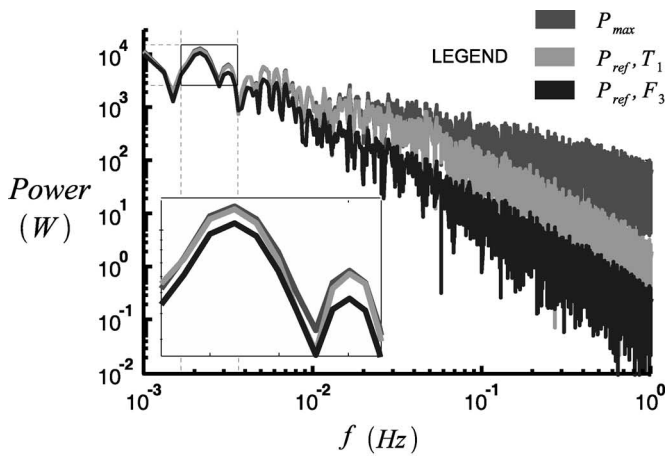

(a)

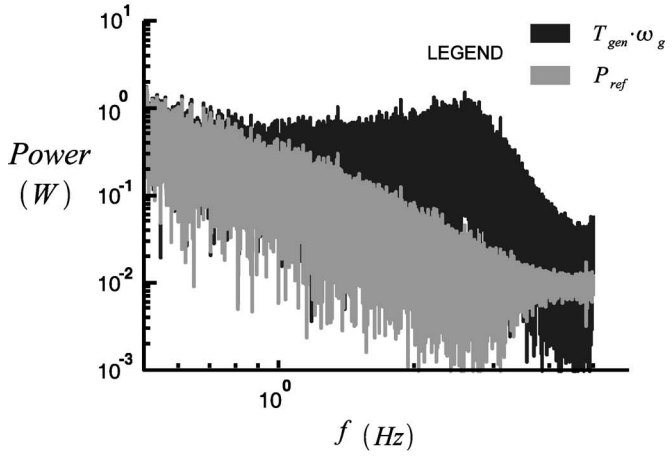

(b)

Fig. 9. Frequency content of power flows. (a) Maximum available wind power and range of possible filtered powers. Filters F_3 and T_1 demonstrate power-filtering and maximum power-tracking in the frequency domain. Inset shows reduced capture at low frequency for F_3 due to derating. (b) Containment of power fluctuations within the conversion system. Delivered power $P_{\rm ref}$ is compared with the generator power. Power variations due to torsional resonance are isolated.

V. RESULTS

Measured wind-time series from the same test site as used in [14] were obtained through a communication with the authors, and employed in all simulations.

A. Adjustable Power-Filter Performance

Fig. 8 shows the delivered power and turbine hub speed over 10 min for power-tracking mode at high efficiency (T_1 in Fig. 6) and for power-filtering mode at derated efficiency (F_3). The

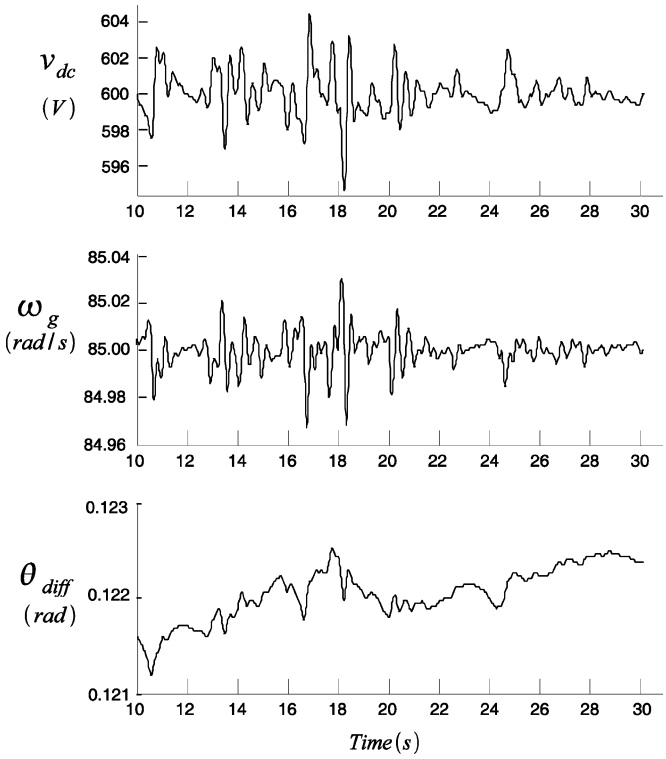

Fig. 10. Regulation of capacitor and torsional oscillations.

maximum available power $P_{\rm max}$ is also plotted. The delivered power clearly tracks $P_{\rm max}$ more closely for the filter T_1. However, the delivered power obtained with the filter F_3 is smoother, though it must be less on average due to its derating. It is evident from the plot of turbine hub speed that this smoothing is possible due to large variations around a higher average speed than that of the filter T_1. A more quantitative demonstration of the tradeoffs of power-filtering mode is provided by the results of several 50-min simulations summarized in Table I. The amount of energy captured relative to the maximum available is shown, as are the filter time constant τ, average speed, and standard deviation of speeds. Operation in filtering mode reduces capture, and higher average speed and larger speed variations are evident from the last two columns. For operation at larger deratings, practical machine speed limits are likely to be reached before the filtering time constant τ reaches the maximum imposed by the aerodynamic stability limit.

B. Containment of Power Variations

Choosing a filtered power $P_{\rm ref}$ attenuates the wind-power variations delivered to the grid. As discussed, the filter time constant must be set within the ability of the turbine hub inertia to absorb fluctuations. Fig. 9 shows the frequency content of delivered power for the optimal power-tracking parameters T_1 and the derated power-filtering parameters F_3.

Specifying $P_{\rm ref}$ based on wind speed rather than on states of the fast subsystem completely removes the influence of those states from the delivered power. Fig. 9(b) compares the generator power with the power $P_{\rm ref}$ delivered to the grid. A hump

in the frequency content of the generator power around 2 Hz corresponds to the torsional resonance [15], [16]. The control structure prevents this torsional resonance from being coupled to power system variables. Variations of the dc-link capacitor voltage and mechanical system states occur due to continual forcing of the torsional resonance by wind disturbances. The effect of the control law defined for $\tilde{T}_{\rm gen}$ on these states is demonstrated in Fig. 10. Variations in the states are well-contained.

VI. Conclusion

As a step toward understanding the limits of imposing a desired power output on wind turbines, a new control structure has been introduced that can cause them to appear as adjustable power filters. It has been shown how this allows a range of operation modes (from power-tracking to power-filtering) over a range of conversion efficiencies. However, a stability limit on the filter time constant used in power-filtering is demonstrated. It was also shown that it is possible to regulate torsional and dc-link voltage dynamics using only the machine-side converter controls, eliminating the influence of internal modes on the grid.

In today's wind installations, providing a filtered power may not yield a monetary value that can compensate the economic losses associated with decreased energy capture. However, in future, problems arising from increased wind-power penetration may drive a need to exploit all the potential operating modes of installed wind turbine generators. For example, a strategy of shifting between optimal power-tracking and a filtered power-extraction mode by adjusting the filter time constant τ and tip-speed ratio λ^* may become useful. A control structure, where delivered power is a control input, is a natural arrangement for implementing new control functions for wind turbines and for studying their impact. Given the growing interest in allowing wind farms to contribute to the regulation of power systems, the methodology and analyses of fundamental limitations presented here warrant further investigation.

References

[1] B. Rabelo and W. Hofmann, "Wind generator control in compliance with new norms," presented at the IEEE Int. Symp. Ind. Electron., Rio de Janeiro, Brazil, Jun. 9–11, 2003.

[2] F. Hughes, O. Anaya-Lara, N. Jenkins, and G. Strbac, "Control of DFIG-based wind generation for power network support," *IEEE Trans. Power Syst.*, vol. 20, no. 4, pp. 1958–1966, Nov. 2005.

[3] F. Koch, I. Erlich, F. Shewarega, and U. Bachmann, "Dynamic interaction of large offshore wind farms with the electric power system," presented at the IEEE Bologna PowerTech Conf., Bologna, Italy, Jun. 23–26, 2003.

[4] T. Gjengedal, "Large scale wind power farms as power plants," *Wind Energy*, vol. 8, no. 3, pp. 361–373, 2005.

[5] L. Ran, J. Bumby, and P. Tavner, "Use of turbine inertia for power smoothing of wind turbines with a DFIG," in *Proc. 11th Int. Conf. Harmonics Quality Power* Sep. 12–15, 2004, pp. 106–111.

[6] C. Sourkounis and B. Ni, "Optimal control structure to reduce the cumulative load in the drive train of wind energy converters," presented at the 11th Eur. Conf. Power Electron. Appl., Dresden, Germany, Sep. 11–14, 2005.

[7] T. Petru, "Modelling of wind turbines for power systems studies" Ph.D. dissertation, Chalmers Univ. Technol., Göteborg, Sweden, Jun. 2003 [Online]. Available: http://www.elkraft.chalmers.se/Publikationer/EMKE.publ/Abstracts/2003/t%omasPhD.html

[8] C. Nichita, D. Luca, B. Dakyo, and E. Ceanga, "Large band simulation of the wind speed for real time wind turbine simulators," *IEEE Trans. Energy Convers.*, vol. 17, no. 4, pp. 523–529, Dec. 2002.

[9] V. Akhmatov, H. Knudsen, and A. Nielsen, "Advanced simulation of windmills in the electric power supply," *Elect. Power Energy Syst.*, vol. 22, pp. 421–434, 2000.

[10] B. C. W. E. Leithead, "Control of variable speed wind turbines: Design task," *Int. J. Control*, vol. 73, no. 13, pp. 1189–1212, 2000.

[11] R. Pena, R. Cardenas, R. Blasco, G. Asher, and J. Clare, "A cage induction generator using back-to-back PWM converters for variable speed grid connected wind energy system," in *IECON'01*, pp. 1376–1381.

[12] H. Khalil, *Nonlinear Systems*. Englewood Cliffs, NJ: Prentice-Hall, 2002.

[13] T. Gjengedal, "Integration of wind power and the impact on power system operation," presented at the Large Eng. Syst. Conf. Power Eng., May 7–9, 2003.

[14] T. Thiringer and J. Dahlberg, "Periodic pulsations from a three-bladed wind turbine," *IEEE Trans. Energy Convers.*, vol. 16, no. 2, pp. 128–133, Jun. 2001.

[15] T. Thiringer, T. Petru, and C. Liljegren, "Power quality impact of a sea located hybrid wind park," *IEEE Trans. Energy Convers.*, vol. 16, no. 2, pp. 123–127, Jun. 2001.

[16] A. Hansen, P. Sorensen, L. Janosi, and J. Bech, "Wind farm modeling for power quality," in *IECON'01*, 2001, pp. 1959–1964.

Barry G. Rawn (S'03) received the B.A.Sc. degree in engineering science and the M.A.Sc. degree in electrical engineering from the University of Toronto, Toronto, ON, Canada, in 2002 and 2004, respectively. He is currently working toward the Ph.D. degree at the Department of Electrical & Computer Engineering, the University of Toronto.

His current research interests include nonlinear dynamics and sustainable energy infrastructure.

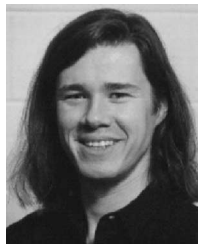

Peter W. Lehn (S'88–M'92–SM'05) received the B.Sc. and M.Sc. degrees from the University of Manitoba, Winnipeg, MB, Canada, in 1990 and 1992, respectively, and the Ph.D. degree from the University of Toronto, Toronto, ON, Canada, in 1999, all in electrical engineering.

From 1992 to 1994, he was with the Network Planning Group of Siemens AG, Erlangen, Germany. Currently, he is an Associate Professor at the University of Toronto.

Manfredi Maggiore (M'00) received the "Laurea" degree in electronic engineering from the University of Genoa, Genoa, Italy, in 1996 and the Ph.D. degree in electrical engineering from the Ohio State University, Columbus, in 2000.

He is currently an Associate Professor in the Edward S. Rogers Sr. Department of Electrical and Computer Engineering, University of Toronto, Toronto, ON, Canada. His current research interests include nonlinear geometric control, magnetic levitation, and control of renewable energy systems.